INTERNATIONAL JOURNAL FOR NUMERICAL METHODS IN ENGINEERING
Int. J. Numer. Meth. Engng 2017; **112**:939–962
Published online 11 April 2017 in Wiley Online Library (wileyonlinelibrary.com). DOI: 10.1002/nme.5538

Finite volume methods for elasticity with weak symmetry

Eirik Keilegavlen[1] and Jan Martin Nordbotten[1,2]

[1]*Department of Mathematics, University of Bergen, Bergen, Norway*
[2]*Department of Civil and Environmental Engineering, Princeton University, Princeton, NJ, USA*

ABSTRACT

We introduce a new cell-centered finite volume discretization for elasticity with weakly enforced symmetry of the stress tensor. The method is motivated by the need for robust discretization methods for deformation and flow in porous media and falls in the category of multi-point stress approximations (MPSAs). By enforcing symmetry weakly, the resulting method has flexibility beyond previous MPSA methods. This allows for a construction of a method that is applicable to simplexes, quadrilaterals, and most planar-faced polyhedral grids in both 2D and 3D, and in particular, the method amends a convergence failure in previous MPSA methods for certain simplex grids. We prove convergence of the new method for a wide range of problems, with conditions that can be verified at the time of discretization. We present the first set of comprehensive numerical tests for the MPSA methods in three dimensions, covering Cartesian and simplex grids, with both heterogeneous and nearly incompressible media. The tests show that the new method consistently is second order convergent in displacement, despite being the lowest order, with a rate that mostly is between 1 and 2 for stresses. The results further show that the new method is more robust and computationally cheaper than previous MPSA methods. Copyright © 2017 The Authors. *International Journal for Numerical Methods in Engineering* Published by John Wiley & Sons Ltd.

Received 25 November 2015; Revised 21 February 2017; Accepted 22 February 2017

KEY WORDS: Finite volume methods; elasticity; weak symmetry; porous media; general grids

1. INTRODUCTION

Fluid flow in porous materials is intrinsically coupled to mechanical stresses induced on the skeleton. In many geological subsurface applications, such as CO_2 storage [1], geothermal energy extraction, for example, [2], and petroleum extraction [3], engineering design calls for high flow rates, and consequently, the induced mechanical stresses become significant. In this context, simulation of coupled flow and deformation in geological porous media is becoming increasingly important.

Numerical simulation of the Biot equations is challenging because of the different mathematical nature of the flow and mechanical equations. In order for stable discretizations to be allowed in the presence of multiple fluid phases, the flow equations are naturally discretized by conservative schemes, such as finite volume methods [4]. In contrast, it is customary to discretize the mechanical equations of equilibrium using finite element methods (FEMs), for example, [5]. This situation has the disadvantage that finite volume and FEMs inherently use different data structures and are best adapted to different grid types. This makes the construction of efficient simulation codes difficult, and as a consequence, fixed-point iteration between disparate computational tools has become industry standard [6].

*Correspondence to: Eirik Keilegavlen, Department of Mathematics, University of Bergen, Bergen, Norway.
†E-mail: Eirik.Keilegavlen@math.uib.no

The status quo for numerical simulation of the Biot equations is not optimal, and several authors have addressed this aspect. Thus, simulation approaches built on finite elements [7, 8], finite differences [9], and finite volumes [6, 10–12] have recently been considered. We argue that in the context of applications related to multiphase flow in geological porous media, it is imperative to use conservative discretizations for the flow equations [13, 14]. As such, we see a need for finite volume methods for mechanics that are designed to handle the grids and material discontinuities typical of industrial reservoir simulation [15–17].

Recently, we proposed a new family of finite volume method for mechanics, referred to as multi-point stress approximation (MPSA) methods [18]. These methods build on the same concepts and the same data structures as the multi-point flux approximation (MPFA) methods common for multiphase flows in porous media [6, 19, 20]. Since introducing the MPSA methods, we have demonstrated their applicability to the coupled Biot system [21].

The class of MPSA methods is qualitatively different from existing cell-centered finite volume discretizations for mechanics. In particular, by building on a discontinuous Galerkin-like structure, they are explicitly formulated to handle discontinuities and anisotropic material properties such as typically encountered in geological applications. In contrast, existing cell-centered finite volume discretizations typically rely on either face values of material properties (see, e.g., the recent paper [22] and the references therein) or smooth interpolations of the displacement field [23, 24]. While the latter approach has recently been extended to handle layered media [25], geological media are often considered to be everywhere heterogeneous, requiring methods that adapt to more complex material structures. This also distinguishes the method from approaches based on control volume finite element approaches [26]. The current work concerns only the discretization of the equations of static linearized elasticity; finite volume methods have been discussed in the context of more dynamics and nonlinear constitutive laws (using reformulation as a coupled set of hyperbolic conservation laws), in other recent work (e.g., [27, 28]).

In the context of locally conservative discretizations for linearized elasticity, we also mention recent work based on finite elements. The idea of weakly imposed symmetry has been used to obtain hybridizable mixed finite element formulations [29]. In this three-field approach, the stress field can be eliminated to obtain a method with cell-centered rotations and displacements. By relaxing the continuity requirements on the spaces, the primal formulation (i.e., displacement variable only) can also be used to derive hybridizable discontinuous Galerkin [30] and hybridizable Crouzeix–Raviart [31] discretizations. In both these cases, methods result which are applicable to a wide range of grids, although with displacement variables located on faces. The finite element-based approaches have the advantage that high-order generalizations are naturally formed (see also recent work on hybridizable high-order methods [32]).

We have recently proved that the MPSA-O method is a convergent discretization for mechanics [33]. The proof highlights the role of local coercivity conditions, which are functions of the local geometry, material parameters, and discretization scheme. These local coercivity conditions can be verified for many classes of grids relevant for applications (Cartesians and so-called PEBI (Perpendicular bisection) or Voronoi grids). However, the situation for simplex grids (triangles in 2D, tetrahedral in 3D) is less clear, and the existing MPSA-type discretizations may fail unless strict conditions of acute angles are enforced on the grids, even in 2D. Thus, the situation is that the MPSA methods until now have been more restrictive in terms of grids than their flow counterpart MPFA.

The existing MPSA methods are all generalizations of their MPFA counterparts, with strong symmetry in the constitutive laws. Herein, we present the first MPSA method, which is explicitly defined to exploit the particular nature of the equations of elasticity. In particular, it is well known in the context of mixed finite elements for elasticity that obtaining inf-sup stable discretizations may require quite sophisticated spaces [34]. On the other hand, imposing symmetry in an integral sense may lead to simpler discretization methods, as studied in the setting of both mixed finite elements [29] and mimetic finite differences [35]. This concept is also referred to as weak symmetry, which is the key tool we will use to obtain the discretization proposed herein.

We are thus motivated by this observation to seek a finite volume discretization with weakly enforced symmetry, particularly tailored to discretization of elasticity. We refer to this new method as MPSA-W, to emphasize that the symmetry is in a weak sense. In exchange for the reduced symmetry, several practical and computational advantages are realized. In particular, the MPSA-W method improves over existing MPSA methods as it (i) avoids solving computationally expensive local

DOI: 10.1002/nme

minimization problems at the time of discretization and (ii) is robust for simplex grids. It shares with existing MPSA discretizations the applicability to general polygonal grids, material discontinuities, and a reasonable robustness with respect to Poisson's ratio. Furthermore, despite the nomenclature, all finite volume methods for elasticity, including the MPSA-W method proposed herein, allow for a post-processing based on local Neumann problems that recovers a point-wise symmetric stress tensor.

We structure the remaining presentation as follows. In Section 2, we first present the governing equations and then introduce the notation necessary to describe the discretization method. The MPSA-W method is then presented in two different settings: Section 3 describes a framework that is natural for implementation, and also shows the similarities with the MPFA counterparts. In Section 4, the method is cast in a discrete variational framework that allows us to discuss the theoretical convergence properties of the method. In Section 5, the performance of the MPSA-W method is assessed by numerical convergence tests in 2D and 3D, before Section 6 provides concluding remarks.

2. EQUATIONS AND GRID

In this section, we introduce the governing equations and notation necessary to describe the discretization schemes.

2.1. Governing equations

We consider the static momentum balance equation for an elastic medium, which in Lagrangian coordinates reads

$$\int_{\partial\Omega} \boldsymbol{T}(\boldsymbol{n}) dA + \int_{\Omega} \boldsymbol{f} dV = 0 \tag{2.1.1}$$

where $\boldsymbol{T}(\boldsymbol{n})$ are the surface traction vectors on the boundary of some domain $\Omega \in R^D D = \{1, 2, 3\}$ with outward facing normal vector $\boldsymbol{n}$ and $\boldsymbol{f}$ represents body forces. Assuming small deformations and a linear stress−strain relation, we can express the surface forces as

$$\boldsymbol{T}(\boldsymbol{n}) = \boldsymbol{\pi} \cdot \boldsymbol{n} = (\mathbb{C} : \boldsymbol{\epsilon}) \cdot \boldsymbol{n} \tag{2.1.2}$$

Here, $\boldsymbol{\pi}$ is the first Piola−Kirchhoff stress tensor, $\mathbb{C}$ is the stiffness tensor, and $\boldsymbol{\epsilon}$ is the symmetric part of the deformation gradient $\boldsymbol{\epsilon} = (\nabla \boldsymbol{u} + (\nabla \boldsymbol{u})^T)/2$. Because we are in the context of small deformations in Euclidian space, the Piola−Kirchhoff stress tensors coincide with the Cauchy stress tensor and are all symmetric.

In the case of an isotropic media, $\mathbb{C}$ can be expressed by the Lamé parameters μ, λ to arrive at the familiar form

$$\boldsymbol{\pi} = 2\mu\boldsymbol{\epsilon} + \lambda \, tr(\boldsymbol{\epsilon})\boldsymbol{I} \tag{2.1.3}$$

When the solution has sufficient smoothness, Equations (2.1.1) and (2.1.2) can be rewritten as the differential equation

$$\nabla \cdot \boldsymbol{\pi} = \boldsymbol{f} \tag{2.1.4}$$

Thus, Equations (2.1.1) and (2.1.3) are equivalent with Equations (2.1.3) and (2.1.4).

2.2. Grid

To define our numerical method for solving (2.1.1)−(2.1.3), we need notation to describe the grid and associated quantities. The notation introduced in the succeeding texts is identical to the one used in [33], as this will allow us to adapt convergence results therein to the weakly symmetric discretization.

We denote a generic cell K, with volume (area in 2D) m_K, and let $\mathcal{T}$ be the set of all cells. Similarly, σ denotes a generic face, with area m_σ, and $\mathcal{F}$ is the set of all faces in the grid. For $D = 3$, we will further denote a generic edge in the grid E. Finally, $\mathcal{V}$ is the set of vertices in the grid, and s will denote a generic vertex.

DOI: 10.1002/nme

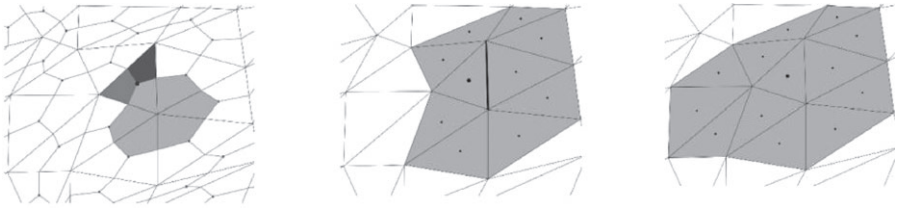

(a) Sub-cells (b) Stress stencil (c) Displacement stencil

Figure 1. Grid structure used in the discretization of the center cell (marked with bullet). (a) Partitioning of triangular cells into subcells: subcells with light gray share the same vertex and form the domain of a local calculation. (b) Stencil for stress discretization on one face. (c) Stencil for displacement discretization for the whole cell.

To simplify the description of the method, we also introduce notation to represent the relation between cells, faces, edges, and vertices. The faces on the boundary of a cell K are denoted F_K, so that $\partial K = \cup_{\sigma\in\mathcal{F}_K}\sigma$, and the vertices of K are $\mathcal{V}_K$. Similarly, for each face, the neighboring cells are denoted $\mathcal{T}_\sigma$ and the face corners $\mathcal{V}_\sigma$. For each vertex $s \in \mathcal{V}$, we denote the adjacent cells by $\mathcal{T}_s$ and the adjacent faces by $\mathcal{F}_s$.

We introduce the following geometric quantities: Let $\boldsymbol{x}_K$ and $\boldsymbol{x}_\sigma$ represent the coordinates of cell and face centers, respectively, and let $\boldsymbol{x}_s$ denote vertex coordinates. For each face, we let $\boldsymbol{n}_{K,\sigma}$ denote the unit normal vector, which is outward facing with respect to the cell $K \in T_\sigma$, and let $d_{K,\sigma}$ be the distance from $\boldsymbol{x}_K$ to $\boldsymbol{x}_\sigma$

Our finite volume method will be constructed to have conservation properties on the cells $\mathcal{T}$. However, much of the construction of the discretization is based on a further partitioning of the cells into subcells; see Figure 1. With each vertex $s \in \mathcal{V}_K$, we associate a subcell that we identify by the pair (s, K), with a volume m_K^s, so that $\sum_{s\in\mathcal{V}_K} m_K^s = m_K$. Similarly, sub-faces are defined for each vertex $s \in \mathcal{V}_\sigma$, identified by the pair (s, σ), and with an area m_σ^s.

With the aforementioned notation, momentum conservation stated for K reads

$$-\int_K \boldsymbol{f}\,dV = \int_{\partial K} \boldsymbol{T}(\boldsymbol{n})\,dA = \sum\nolimits_{\sigma\in\mathcal{F}_K} \boldsymbol{T}_{K,\sigma} \tag{2.2.1}$$

where $\boldsymbol{T}_{K,\sigma}$ denotes the forces acting on σ.

3. DISCRETIZATION

This section is devoted to the introduction of MPSA methods with both weak and strong symmetries. The presentation and notation in this section are convenient for implementation, while Section 4 offers an alternative notation that is better suited for convergence analysis.

3.1. Discrete variables

We discretize the displacements in terms of cell-center displacements and denote these degrees of freedom $\boldsymbol{u}_K$. To each cell K, and for each component of the displacement vector, we further associate basis functions, which are piecewise linear functions on each subcell, and with support on all subcells for which $\boldsymbol{x}_K$ is a vertex; see Figure 1a. The gradients that define the basis functions of cell K are denoted $\boldsymbol{G}_K$, and together with $\boldsymbol{u}_K$, they define the discrete displacements everywhere. To obtain a global discretization in terms of cell-center displacements, the gradients must be eliminated by local calculations. Before we carry out the elimination, it is therefore necessary to introduce the discretized tractions on the surface and in particular introduce the notion of weakly enforced symmetry of the stress tensor.

DOI: 10.1002/nme

3.2. Discrete representation of face stresses

In the continuous setting, the stress at a point is given by $\boldsymbol{\pi} = \mathbb{C}_K : \boldsymbol{\epsilon}(\boldsymbol{u})$. The discrete analogue can be written in terms of the discrete gradients $\boldsymbol{G}_K^s$ as

$$\underline{\boldsymbol{\pi}}_{K,s} = \frac{\mathbb{C}_K : \boldsymbol{G}_K^s + \left(\mathbb{C}_K : \boldsymbol{G}_K^s\right)^T}{2} \tag{3.2.1}$$

where we have exploited that $\mathbb{C}_K$ can be written as a symmetric tensor. This discrete stress expression (3.2.1) was introduced in [18] and leads to the MPSA-O methods with strong symmetry (emphasized by the underscore).

The purpose of this paper is to explore alternative discrete formulations of stresses, leading to methods with weak symmetry. We will see that this method has superior qualities for practical computations. To this end, the discretized term $\mathbb{C}_K : \boldsymbol{G}_K^s - \left(\mathbb{C}_K : \boldsymbol{G}_K^s\right)^T$, which represents the asymmetric component of the stress tensor, is replaced by a quantity averaged over the surrounding subcells. Specifically, we introduce two notions of weak symmetry: one is associated with vertices of the grid, while the second is associated with edges of the grid. These notions coincide in 2D but lead to distinct methods in 3D. It is important to note that because of the continuity of tractions (as opposed to strain), this weak imposition of symmetry does not smear out material contrasts.

We introduce the notation for the average associated with vertices, $\langle\cdot\rangle_s$, and define the discrete stress with symmetry weakly imposed in the neighborhood of vertices as

$$\boldsymbol{\pi}_{K,s} = \mathbb{C}_K : \boldsymbol{G}_K^s - \frac{\langle\mathbb{C}_k : \boldsymbol{G}_K^s\rangle_s - \langle\mathbb{C}_k : \boldsymbol{G}_K^s\rangle_s^T}{2} \tag{3.2.2}$$

We observe that the first term on the right is in general not symmetric and that the second term subtracts the asymmetric part of the stress tensor. The term weak symmetry is justified because

$$\langle\boldsymbol{\pi}_{K,s} - \boldsymbol{\pi}_{K,s}^T\rangle_s = \langle\mathbb{C}_K : \boldsymbol{G}_K^s - (\mathbb{C}_K : \boldsymbol{G}_K^s)^T - \langle\mathbb{C}_K : \boldsymbol{G}_K^s\rangle_s + \langle\mathbb{C}_K : \boldsymbol{G}_K^s\rangle_s^T\rangle_s = 0$$

by linearity of the averaging operator and because $\langle\langle\mathbb{C}_K : \boldsymbol{G}_K^s\rangle_s\rangle_s = \langle\mathbb{C}_K : \boldsymbol{G}_K^s\rangle_s$.

While edges and vertices coincide in 2D, they are distinct in 3D. A slightly stronger notion of symmetry can thus be enforced at the expense of the additional data structure needed to handle edges. We introduce the notation for edge average $\langle\cdot\rangle_e$ and introduce the discrete stress with symmetry weakly imposed around edges as

$$\boldsymbol{\pi}_{K,s,e} = \mathbb{C}_K : \boldsymbol{G}_K^s - \frac{\langle\mathbb{C}_k : \boldsymbol{G}_K^s\rangle_e - \langle\mathbb{C}_k : \boldsymbol{G}_K^s\rangle_e^T}{2} \tag{3.2.3}$$

Again, the term weak symmetry is justified as shown earlier. We will refer to the stress discretization (3.2.2) as the MPSA-W method with vertex-wise averaging, while (3.2.3) will be termed edge-wise averaging; in 2D, we will simply refer to the MPSA-W method. We note that both vertex-wise and edge-wise averaging is dependent on the material model having an explicit representation of $\mathbb{C}_K$. We also note that the formulations (3.2.2) and (3.2.3) are similar to the way symmetry can be weakly enforced for mixed FEMs. We will return to this matter in Section 4.2.

Based on any of the discrete stresses $\boldsymbol{\chi}_{K,s,e} = \{\underline{\pi}_{K,s}\pi_{K,s}\pi_{K,s,e}\}$, we can define discrete tractions according to

$$\boldsymbol{T}_{K,s}^{\sigma} = \sum\nolimits_{e\in\varepsilon_s\cap\varepsilon_\sigma} m_\sigma^{s,e}\boldsymbol{\chi}_{K,s,e}\cdot\boldsymbol{n}_{K,\sigma} \tag{3.2.4}$$

3.3. Local linear system

Independent of which discretization of stress is chosen, the finite volume framework requires that the stress over a sub-face is continuous, that is,

$$\boldsymbol{T}_{R,s}^{\sigma} = -\boldsymbol{T}_{L,s}^{\sigma}, \qquad \text{with } \{R,L\} = \mathcal{T}_\sigma \tag{3.3.1}$$

DOI: 10.1002/nme

We note that via the definition of discrete tractions (3.2.1)-(3.2.3), this is an equation for gradients $\boldsymbol{G}_K^s$. For implementation purposes, it is important to note that by construction, the term

$$\langle \mathbb{C}_K : \boldsymbol{G}_K^s \rangle_s^T \cdot \boldsymbol{n}_{K,\sigma} = -\langle \mathbb{C}_K : \boldsymbol{G}_L^s \rangle_s^T \cdot \boldsymbol{n}_{L,\sigma} \tag{3.3.2}$$

(and similarly for the average over e), thus only the non-transpose part $\mathbb{C} : \boldsymbol{G}_K^s$, will contribute to (3.3.1). This is significant, because this gives a locally coercive system, in turn allowing for a significantly simpler method than that of strong symmetry in the discrete stress tensor.

We will also require certain continuity properties for the displacement: For each sub-face (s, σ), we impose displacement continuity in a point $\boldsymbol{x}_{\sigma,C}^s = \eta \boldsymbol{x}_s + (1-\eta)\boldsymbol{x}_\sigma$. Here, η is a parameter, which in general can be chosen to optimize the method. For simplex grids, geometric identities imply that the choice of $\eta = 1/3$ will lead to symmetries in the discretization (in the notation of Equations (4.1.2) and (4.1.3) shown later, this choice leads to $\boldsymbol{g}_{K,\sigma}^s = \boldsymbol{n}_{K,\sigma}$), which have proved to be favorable for the related MPFA discretizations; however, for other grids, the choice $\eta = 0$ is a reasonable compromise [36, 37].

For each face, the continuity requirement gives an equation

$$\boldsymbol{u}_R + \boldsymbol{G}_R^s \left(\boldsymbol{x}_{\sigma,C}^s - \boldsymbol{x}_R \right) = \boldsymbol{u}_L + \boldsymbol{G}_L^s \left(\boldsymbol{x}_{\sigma,C}^s - \boldsymbol{x}_L \right), \quad \text{with } \{R, L\} = \mathcal{T}_\sigma \tag{3.3.3}$$

Note that the use of a single continuity point leads to the MPSA-O method when using the symmetric discrete stress $\underline{\pi}_{K,s}$. However, this method is only applicable to simplex grids; thus, the *generalized* MPSA-O method (with a minimization problem for discontinuities) is used for general grids [18]. The MPSA-W method avoids this additional complexity, and we will limit the presentation to this simpler case.

While (3.3.3) enforces a certain displacement continuity between subcells located in different cells, we require no such continuity between subcells contained within a single cell K. This is a key component of the MPSA methods, which allows us to write the gradients $\boldsymbol{G}_K^s$ in terms of cell-center displacements in Equation (3.2.4) by a local calculation, involving only subcells surrounding a single vertex. To be specific, the stress continuity (3.3.1) and the displacement continuity (3.3.3) can be combined into a linear system, which represents local calculations for each corner. These local systems can be thought of as analogues to approaches based on resolved multiscale basis functions [38, 39]

$$\begin{pmatrix} \boldsymbol{S}_G & \boldsymbol{0} \\ \boldsymbol{D}_G & \boldsymbol{D}_U \\ \boldsymbol{0} & \boldsymbol{I} \end{pmatrix} \begin{pmatrix} \boldsymbol{G} \\ \boldsymbol{U} \end{pmatrix} = \begin{pmatrix} \boldsymbol{0} \\ \boldsymbol{0} \\ \boldsymbol{I} \end{pmatrix} \tag{3.3.4}$$

Here, $\boldsymbol{S}_G$ represents products on the form $\boldsymbol{n}^T\mathbb{C}$, $\boldsymbol{D}_G$ contains distances from cell centers to continuity points, $\boldsymbol{D}_U$ is a matrix of ± 1 representing the contributions from cell centers in (3.3.3), while $\boldsymbol{I}$ is the identity matrix. The unknowns are all gradients in the subcells ($\boldsymbol{G}$) and all cell-center displacements ($\boldsymbol{U}$). The first two rows in (3.3.4) thus represent continuity of forces and displacement. Each row in the lower block enforces a unit displacement in one cell center at a time; thus, (3.3.4) must be solved for $D|\mathcal{T}_s|$ right-hand sides, with $|\mathcal{T}_s|$ denoting the number of cells in $\mathcal{T}_s$. When the solution $\boldsymbol{G}$ is inserted into (3.2.4), we obtain the desired expressions for surface forces on a sub-face in terms of cell-center displacements.

The unique solvability of Equation (3.3.4) is an important aspect of the method. By counting degrees of freedom and equations, we see that they match only if the number of cell faces that meet in a vertex equals 2 in 2D and 3 in 3D. The method in its current formulation is therefore not defined for more general polyhedra, such as pyramids, although such extensions may be possible following related work for the scalar equation [40]. We will return to the solvability of (3.3.4) in more detail in Section 4.

Boundary conditions are incorporated into (3.3.4) by adjusting (3.3.1) (for Neumann conditions), (3.3.3) (Dirichlet conditions), or a combination thereof (mixed conditions).

DOI: 10.1002/nme

3.4. Global linear system

The local calculation is carried out for all faces in the grid to obtain discrete traction in terms of the surrounding displacements, which we will write on the form $\boldsymbol{T}^{\sigma}_{K,s} = \sum_{K' \in \mathcal{T}_s} t_{K,K',s,\sigma}\, \boldsymbol{u}_{K'}$. Here $t_{K,K',s,\sigma}$ are the second-order tensor coefficients of the discrete Hooke's law and thus express the discrete representation of the differential operator and the stiffness tensor. Insertion into (2.1.2) now gives

$$-\int_K \boldsymbol{f} dV = \sum_{\sigma \in \mathcal{F}_K} \boldsymbol{T}_{K,\sigma} = \sum_{\sigma \in \mathcal{F}_K} \sum_{s \in \mathcal{V}_\sigma} \boldsymbol{T}^{\sigma}_{K,s} = \sum_{\sigma \in \mathcal{F}_K} \sum_{s \in \mathcal{V}_\sigma} \sum_{K' \in \mathcal{T}_s} t_{K,K',s,\sigma}\, \boldsymbol{u}_{K'} \tag{3.4.1}$$

This expresses force balance on cell K as a linear combination of the displacements of all cells K' that share at least one vertex s with K, with the sums taken over all the faces of K. When (3.4.1) is assembled for all $K \in T$, and boundary conditions are taken into account, this results in a linear system for the cell-center displacements.

For the tests reported herein, system (3.4.1) is solved either with a direct solver as implemented by Matlab's backslash operator or for the larger systems, GMRES preconditioned with ILU(0).

4. THEORETICAL CONSIDERATIONS

Convergence of the generalized MPSA-O method with strong symmetry has been proved, conditional on locally computable criteria relating to grid and material parameters [33]. We will cast the MPSA-W method in the same framework. However, we will see that the local criteria are different and indeed favor the MPSA-W method over the MPSA-O methods. Furthermore, we see that the MPSA-W method has a potential link to mixed FEMs that appears not to be possible for earlier methods with strong symmetry.

4.1. Convergence in the discrete variational framework

Equations (3.2.4) and (3.4.1) are equivalent to a discrete variational form. Indeed, let us consider the function space $\boldsymbol{\mathcal{H}}_T$ consisting of cell-center displacements and the space $\boldsymbol{\mathcal{H}}_C$ consisting of cell-center displacements as well as displacements at the face centers [33, 40, 41]. On the space $\boldsymbol{\mathcal{H}}_C$, we can define a gradient that is consistent with a planar interpolation between the cell-center variables and the face-center variables:

$$\left(\overline{\nabla}\boldsymbol{u}\right)^s_K = \sum\nolimits_{\sigma \in \mathcal{F}_K \cap \mathcal{F}_s} \left(\langle \boldsymbol{u} \rangle^{\sigma}_{K,s} - \boldsymbol{u}_K\right) \otimes \boldsymbol{g}^s_{K,\sigma} \tag{4.1.1}$$

The vectors $\boldsymbol{g}^s_{K,\sigma}$ are uniquely defined in 2D and for most 3D grids (where the restriction for each cell is that no more than three of its faces meet at a vertex [40]) by the equations

$$\boldsymbol{I} = \left(\overline{\nabla}\boldsymbol{x}\right)^s_K = \sum\nolimits_{\sigma \in \mathcal{F}_K \cap \mathcal{F}_s} \left(\langle \boldsymbol{x} \rangle^{\sigma}_{K,s} - \boldsymbol{x}_K\right) \otimes \boldsymbol{g}^s_{K,\sigma} \tag{4.1.2}$$

We see from Equation (3.3.3) that this gradient is consistent with $\boldsymbol{G}^s_K$. In order to enforce a conservation principle, we additionally utilize a gradient built from the normal vectors of the grid and that corresponds to a divergence in the variational framework:

$$\left(\widetilde{\nabla}\boldsymbol{u}\right)^s_K = \frac{1}{m^s_K} \sum\nolimits_{\sigma \in \mathcal{F}_K \cap \mathcal{F}_s} m^s_\sigma \left(\langle \boldsymbol{u} \rangle^{\sigma}_s - \boldsymbol{u}_K\right) \otimes \boldsymbol{n}_{K,\sigma} \tag{4.1.3}$$

With these two discrete gradient operators, we can rewrite the finite volume method for elasticity as a variational problem by introducing the bilinear form $(\boldsymbol{u}, \boldsymbol{v}) \in \boldsymbol{H}_C \times \boldsymbol{H}_C$

$$b_{\mathcal{D}}(\boldsymbol{u}, \boldsymbol{v}) = \sum\nolimits_{K \in \mathcal{T}} \sum\nolimits_{s \in \mathcal{V}_K} m^s_K \left[\mathbb{C}_K : \left(\overline{\nabla}\boldsymbol{u}\right)^s_K - \frac{\langle \mathbb{C}_K : (\overline{\nabla}\boldsymbol{u})^s_K \rangle_x - \langle \mathbb{C}_k : (\overline{\nabla}\boldsymbol{u})^s_K \rangle^T_x}{2} \right] : \left(\widetilde{\nabla}\boldsymbol{v}\right)^s_K \tag{4.1.4}$$

DOI: 10.1002/nme

Recall that $\langle \mathbb{C}_K : (\overline{\nabla}\boldsymbol{u})^s_K \rangle_x$ corresponds to the average stress around vertex or edge, with $x \in \{s, e\}$. The equivalent variational problem to Equations (3.2.4) and (3.4.1) is then stated as follows: Find $\boldsymbol{u}_\mathcal{D} \in \boldsymbol{\mathcal{H}}_\mathcal{C}$ such that

$$b_D(\boldsymbol{u}_D, \boldsymbol{v}) = \int_\Omega \boldsymbol{f} \cdot \mathcal{P}_{\mathcal{C},\mathcal{T}} \boldsymbol{v} \, d\boldsymbol{x} \qquad \text{for all } \boldsymbol{v} \in \boldsymbol{\mathcal{H}}_C \tag{4.1.5}$$

Here, $\mathcal{P}_{\mathcal{C},\mathcal{T}}$ is the projection of $\boldsymbol{\mathcal{H}}_\mathcal{C}$ onto piecewise constants on the cells. Equivalence between the finite volume formulation in (3.2.4) and (3.4.1) and the variational formulation in Equation (4.1.5) is verified by considering the canonical basis for the test functions $\boldsymbol{v}$ [33, 40]. It is particularly useful to split Equation (4.1.5) into two components, in the spirit of a variational multiscale method [42] associated with the cell-center space $\boldsymbol{\mathcal{H}}_\mathcal{T}$ and the cell-face space $\boldsymbol{\mathcal{H}}_\mathcal{F} = \boldsymbol{\mathcal{H}}_\mathcal{C}/\boldsymbol{\mathcal{H}}_T$: Find $(\boldsymbol{u}_\mathcal{T}, \boldsymbol{u}_\mathcal{F}(\boldsymbol{u}_\mathcal{T})) \in \boldsymbol{\mathcal{H}}_\mathcal{T} \times \boldsymbol{\mathcal{H}}_\mathcal{F}$ such that

$$b_\mathcal{D}(\boldsymbol{u}_\mathcal{T} + \boldsymbol{u}_\mathcal{F}(\boldsymbol{u}_\mathcal{T}), \boldsymbol{v}) = \int_\Omega \boldsymbol{f} \cdot \mathcal{P}_{\mathcal{C},\mathcal{T}} \boldsymbol{v} \, d\boldsymbol{x} \qquad \text{for all } \boldsymbol{v} \in \boldsymbol{\mathcal{H}}_\mathcal{T} \tag{4.1.6}$$

$$b_\mathcal{D}(\boldsymbol{u}_\mathcal{F}(\boldsymbol{u}_\mathcal{T}), \boldsymbol{v}) = -b_\mathcal{D}(\boldsymbol{u}_\mathcal{T}, \boldsymbol{v}) \qquad \text{for all } \boldsymbol{v} \in \boldsymbol{\mathcal{H}}_\mathcal{F} \tag{4.1.7}$$

The point is, as noted in Section 3.3, that Equation (4.1.7), and thus the calculation of the projection operators $\Pi_{FV}\boldsymbol{u}_\mathcal{T} = \boldsymbol{u}_\mathcal{T} + \boldsymbol{u}_\mathcal{F}(\boldsymbol{u}_\mathcal{T})$, can be resolved locally around each vertex of the grid. Thus, Equation (4.1.6) represents the finite volume method with degrees of freedom in the cell centers only.

In order to invoke the convergence results of [33], we need that the local systems (4.1.7) used to calculate $\boldsymbol{\Pi}_{FV}$ have a unique solution. In general, this appears to always hold true in practice [40, 43]; however, the proof is elusive even in the case of the scalar MPFA-O method. Here, we thus verify that the local problems for the MPSA-W method are essentially equivalent to the MPFA-O method. This ensures that the methods will have similar grid restrictions, following the motivation from the introduction that the discretizations for flow and mechanics should be compatible.

Lemma 4.1
Let $\lambda = 0$. Then the local problems (4.1.7) for the MPSA-W methods are equivalent to those of the MPFA-O method.

Proof
Because of (3.3.2), the local problems for the case of $\lambda = 0$ are nothing but three independent scalar problems; each of which is equivalent to the MPFA-O methods.

□

It is important to note that this relationship does not hold for the MPSA-O method with strong symmetry, because we then do not have (3.3.2). This necessitated the development of the generalized MPSA-O method [18], for which Lemma 4.1 can be proved (also for nonzero λ) because of the existence of a minimization problem. Thus, obtaining Lemma 4.1, while retaining a simple discretization without local minimization problems, is one of the main advantages of the method proposed herein.

The practical quality of the discretization depends on the bilinear forms are sufficiently close to being symmetric within the subspace defined by the solution to the local problems. We denote by $b_{\mathcal{D},s}$ and $\boldsymbol{\Pi}_{FV,s}$ the restriction of the bilinear form and the projection operator to the cells $K \in \mathcal{T}_s$, respectively:

Local coercivity condition: For every vertex $s \in \mathcal{V}$, there exists a constant $\theta_s \geqslant \theta > 0$ such that the bilinear form $b_{\mathcal{D},s}$ and the projection $\boldsymbol{\Pi}_{FV,s}$ satisfy for all $\boldsymbol{u} \in \Pi_{FV,s}\boldsymbol{\mathcal{H}}_\mathcal{T}/\mathfrak{R}(\Omega)$, where $\mathfrak{R}(\Omega)$ denotes the rigid body motions on Ω

$$b_{\mathcal{D},s}(\boldsymbol{u}, \boldsymbol{u}) \geqslant \theta_s \, |\boldsymbol{u}|^2_{b_{\mathcal{D},s}}$$

DOI: 10.1002/nme

where the local energy semi-norm is associated with the symmetrized bilinear form

$$|\boldsymbol{u}|^2_{b_{\mathcal{D},s}} = \sum_{K\in\mathcal{T}_s} m^s_K \boldsymbol{\epsilon}^s_K : \mathbb{C} : \boldsymbol{\epsilon}^s_K$$

This assumption can be verified locally while assembling the discretization. We will return to both the solvability of the local system, Lemma 4.1, as well as the local coercivity condition, in the Results section.

We point out that the local coercivity condition on this form is an inherent feature of these types of methods and appears for both the MPSA-O method discretization [33] and all convergence proofs for the MPFA-type methods for scalar equations (e.g., [40, 44]). However, as mentioned also in these references, because the coercivity condition is locally computable, it can be verified directly at the time of discretization, and corrective measures, such as local grid refinement, can be applied if necessary [45].

Given the solvability of the local problems and the local coercivity condition, convergence of the method follows directly from previous analysis [33]. In the interest of the exposition being self-contained, we nevertheless recall the three main results, with summary of the main elements of the proof:

Theorem 4.2
For given parameter field $\mathbb{C}$ and mesh $\mathcal{D}$, let the local coercivity condition hold. Then the coarse variational problem (4.1.6) is coercive in the sense that it satisfies if (i) $\boldsymbol{\Gamma}_D$ is measurable then for all $\boldsymbol{u} \in \boldsymbol{\mathcal{H}}_{\mathcal{T}}$ and (ii) if $\Gamma_N = \partial\Omega$ then for all $\boldsymbol{u} \in \boldsymbol{\mathcal{H}}_{\mathcal{T}}/\boldsymbol{\mathfrak{R}}(\Omega)$

$$b_{\mathcal{D}}\left(\Pi_{FV}\boldsymbol{u}, \Pi_{\mathcal{C}}\left(\Pi_{FV}\boldsymbol{u}\right)\right) \geqslant \Theta\, |u|^2_{\mathcal{T}}$$

where the constant $\boldsymbol{\Theta}$ is dependent on the properties of the mesh D and the constant θ but does not scale with h.

Outline of proof. In addition to summation over the local coercivity condition, a discrete Korn's inequality is needed. This is obtained by interpreting the finite volume solution in terms of a linear discontinuous Galerkin discretization on subcells [33], for which Korn's inequality is known to hold [46, 47].

Lemma 4.3
Let D_n be a family of regular discretization triplets (in the sense that mesh shape parameters remain bounded) such that $h_n \to 0$, as $n \to \infty$. Furthermore, let $\boldsymbol{\Theta}$ be bounded independently of n. Then for all n, the solutions $\boldsymbol{u}_n$ of Equation (4.1.6) exist and are unique; there exists $\tilde{u} \in (H_1(\Omega))^d$; and up to a subsequence (still denoted by n), $\Pi_{\mathcal{T}}\boldsymbol{u}_n \to \tilde{u}$ converges in $(L^q(\Omega))^d$, for $q \in [1, 2d/(d-2+\epsilon))$ as $h_n \to 0$. Furthermore, the cell averages of the gradients $\overline{\nabla}_{\mathcal{D}}\boldsymbol{u}_n$ and $\tilde{\nabla}_{\mathcal{D}}\boldsymbol{u}_n$ converges strongly and weakly, respectively, to $\nabla\tilde{u}$ in $\left(L^2(\Omega)\right)^{d^2}$.

Outline of proof. The proof relies on the coercivity of the discretization, Theorem 4.2, as well as the compactness results known for hybrid variational finite volume methods [40, 41]. The strong convergence of $\overline{\nabla}_{\mathcal{D}}\boldsymbol{u}_n$ also builds on the local coercivity condition.

Theorem 4.4
Consider the same case as in Lemma 4.3. Then the limit $\tilde{u} \in \left(H^1(\Omega)\right)^d$ of the discrete mixed variational problem (4.1.6), and consequently the MPSA W-method, is the unique weak solution of Equations (2.1.3) and (2.1.4).

Outline of proof. In addition to Theorem 4.2 and Lemma 4.3, we require consistency of the discretization. The key observation is the strong and weak convergence of $\overline{\nabla}_{\mathcal{D}}\boldsymbol{u}_n$ and $\tilde{\nabla}_{\mathcal{D}}\boldsymbol{u}_n$, respectively, such that the product in (4.1.4) is convergent.

DOI: 10.1002/nme

4.2. Relationship to mixed finite element methods

It is known that for discretization of the Darcy flow equation, there is a relationship between the MPFA method and mixed FEMs. In particular, one may interpret the solution of the local problems given in (3.3.4) in the sense of a broken RT0 space [44] after which a stable and convergent mixed FEM can be defined using piecewise constant functions for the pressure. A similar argument can be made by exploiting BDM1−P0 spaces [48]. Both of these relationships rely on localizing the integrals in the mixed method through the use of appropriately chosen quadrature rules [49, 50].

For the discretization of elasticity through Equations (2.1.3) and (2.1.4), the situation is less clear than in the scalar case. This is due to the difficulty of constructing simple mixed FEMs for elasticity. Indeed, as it seems clear that there are no simple mixed FEMs for elasticity utilizing the Hellinger−Reissner functional [34], thus there is no direct mixed finite element equivalent to the existing MPSA methods with strong symmetry. Therefore, previous analysis of the MPSA-O method has exploited the interpretation of the local problems (3.3.4) in terms of discontinuous Galerkin discretization [18, 46].

In contrast, there exist simple discretizations for elasticity with weakly imposed symmetry [28, 44]. Lowest-order variants of these discretizations use the BDM1 spaces for the components of stress and P0 for displacements. The simplest possible spaces for rotations are P0 [44], corresponding to cell-wise enforcement of weak symmetry. With this, it is not straightforward to simplify the resulting discretizations to a finite volume method in terms of only displacement variables. In contrast, if the rotation spaces are chosen as P1 [44], corresponding to weak symmetry around vertices, it may be possible to construct quadrature rules that result in finite volume methods similar to the MPSA-W method presented herein. Research in this direction is currently ongoing.

4.3. Comparison with earlier multi-point stress approximation methods

The construction given in Section 3, as well as the analysis tools given in Section 4.1, allows us to give a qualitative comparison between the proposed MPSA methods. A quantitative comparison will follow in the Results section.

First, we note that in analogy to the MPFA methods, the so-called MPSA-U and MPSA-L methods can also be constructed [18]. However, these do not have a unique pointwise interpretation of stress and consequently suffer from numerical locking for high Poisson's ratios and are not amenable to the analysis framework of Section 4.1. These methods are considered inferior in the context of elasticity and will not be discussed further herein.

The MPSA-O method with strong symmetry does not lead to local problems with a unique solution given a single continuity point per face as in Equation (3.3.3) except on simplex grids with acute angles. To rectify this deficiency, a richer space of face variables needs to be introduced, where continuity is enforced weakly [18, 33], and the local linear system takes the form of a constrained minimization problem. The resulting method is termed the generalized MPSA-O method. This method is largely locking-free (except on PEBI grids) and shows good convergence properties. However, for simplex grids, the local coercivity condition does not in general hold, and the method performs relatively poorly on these grids. A particularly striking example arises on equilateral simplex grids, where the MPSA-O method is not locally coercive, while the MPSA-W method is. The loss of coercivity for the MPSA-O method is associated with the displacement pattern illustrated in Figure 2, because all the motions are locally rigid body motions, while (to lowest order) continuous at grid faces. Because the MPSA-W method only enforces symmetry weakly, this solution is not in the null space of $b_{\mathcal{D}}$ as defined in Equation (4.1.4).

The MPSA-W method proposed herein has a unique solution to the local problems under similar conditions to the MPFA-O, because they both have essentially equivalent locally coercive operators for the fine-scale problems. In practice, no examples have been found where the local problems do not have a unique solution, and as such, there is no need to introduce the weak displacement continuity used to obtain the generalized MPSA-O method. Consequently, the method is significantly simpler, with much smaller local problems. We have verified that should a case be found where the local problems are singular for the MPSA-W method, this can be handled by introducing multiple

DOI: 10.1002/nme

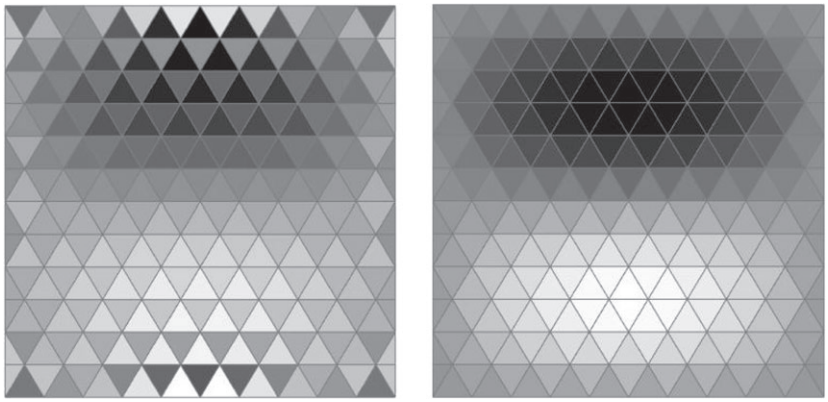

Figure 2. Oscillations due to loss of coercivity for the MPSA-O method. The local oscillations shown to the left persist under grid refinement. (a) Numerical solution and (b) exact solution.

continuity points in (3.3.3) for this local problem, effectively constructing a generalized MPSA-W method.

An important observation in the analysis of MPFA and MPSA methods on simplex grids is that for the single continuity point chosen as O(1/3) (as defined in Section 3.3), the operators $\overline{\nabla}$ and $\tilde{\nabla}$ coincide [37, 40]. For the MPFA-O method, this implies symmetry, and moreover, the local coercivity condition is trivially satisfied. For the MPSA-W method, the same holds for homogeneous materials, and the method is therefore suitable for arbitrary simplex grids for homogeneous problems. None of the previous MPSA methods share this property.

5. NUMERICAL EXPERIMENTS

In this section, the performance of the MPSA-W method is compared with that of the generalized O-method. The quality measurements we consider are errors and convergence properties, computational cost, and accuracy of the angular momentum on cells.

An implementation of the MPSA-W method with vertex-wise averaging, using the Matlab Toolbox, can be downloaded from [51].

5.1. Convergence

To verify the performance of the MPSA-W method, we consider numerical examples that test the performance of the methods on homogeneous and heterogeneous problems in 2D and 3D. We consider Cartesian and simplex grids and test both smooth grids and rough perturbations, as illustrated in Figure 3a. To limit the influence of random perturbations, all variations of methods and material parameters are performed on the same perturbed grids.

5.1.1. Numerical setup. We first consider the unit square with a heterogeneity upper right corner, defined by the characteristic function

$$\chi_{2D}(x,y) = \begin{cases} 1, & \min(x,y) > 1/2 \\ 0, & \text{otherwise} \end{cases} \tag{5.1.1}$$

The material parameters are then defined as $\mu = \left(1 - \chi_{2D}\right) + \kappa\chi_{2D}$ and $\lambda = \alpha\mu$; high values of α correspond to a nearly incompressible material. For this medium, we consider the analytical solution

$$\boldsymbol{u}(x,y) = \begin{pmatrix} (x-0.5)^2(y-0.5)^2 \\ -\frac{2}{3}(x-0.5)(y-0.5)^3 \end{pmatrix} / \left(\left(1-\chi_{2D}\right) + \kappa\chi_{2D}\right) \tag{5.1.2}$$

DOI: 10.1002/nme

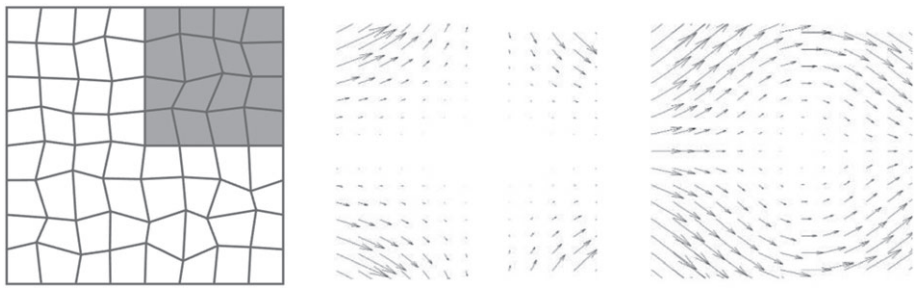

Figure 3. Representative grid (a), solution (b), and body force (c) for the 2D problem in the homogeneous case ($\kappa = 1$). The gray area in (a) indicates the parameter heterogeneity.

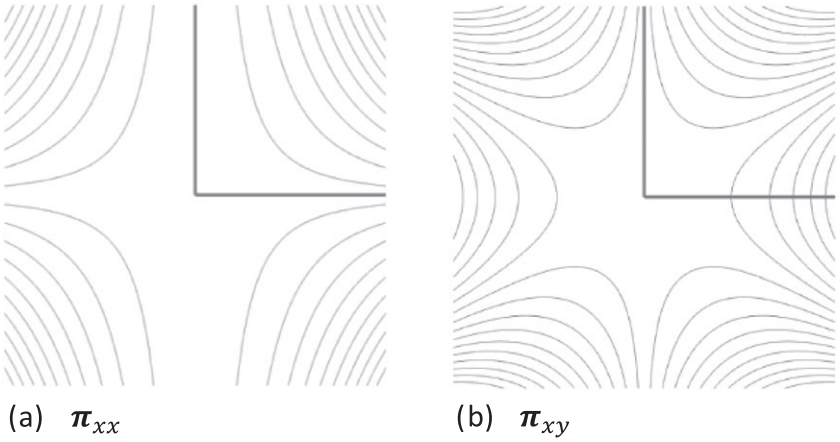

Figure 4. Contours of xx and xy components of the stress tensor. The stress is continuous over the heterogeneity, indicated by thick black lines. (a) π_{xx} and (b) π_{yx}.

The solution is depicted in Figure 3 together with the body force, which is found by taking the divergence of the stress. Boundary conditions are defined are defined according to the analytical solution. Note that the analytical solution is constructed so that the stress field is independent of the material heterogeneity, as illustrated by Figure 4.

We construct a similar three-dimensional solution on the unit cube. Again, we place a heterogeneity upper right corner, this time defined by the characteristic function

$$\chi_{3D}(x,y,z) = \begin{cases} 1, & \min(x,y,z) > 1/2 \\ 0, & \text{otherwise} \end{cases} \tag{5.1.3}$$

The material parameters are then defined as $\mu = (1 - \chi_{3D}) + \kappa\chi_{3D}$ and $\lambda = \alpha\mu$. For this medium, we consider the analytical solution

$$\boldsymbol{u}(x,y,z) = \begin{pmatrix} (x-0.5)^2(y-0.5)^2(z-0.5)^2 \\ (x-0.5)^2(y-0.5)^2(z-0.5)^2 \\ -\frac{2}{3}((x-0.5)(y-0.5)^2 + (x-0.5)^2(y-0.5))(z-0.5)^3 \end{pmatrix} / ((1-\chi_{3D}) + \kappa\chi_{3D}) \tag{5.1.4}$$

This analytical solution is divergence free, with a stress field that is independent of the material heterogeneity.

DOI: 10.1002/nme

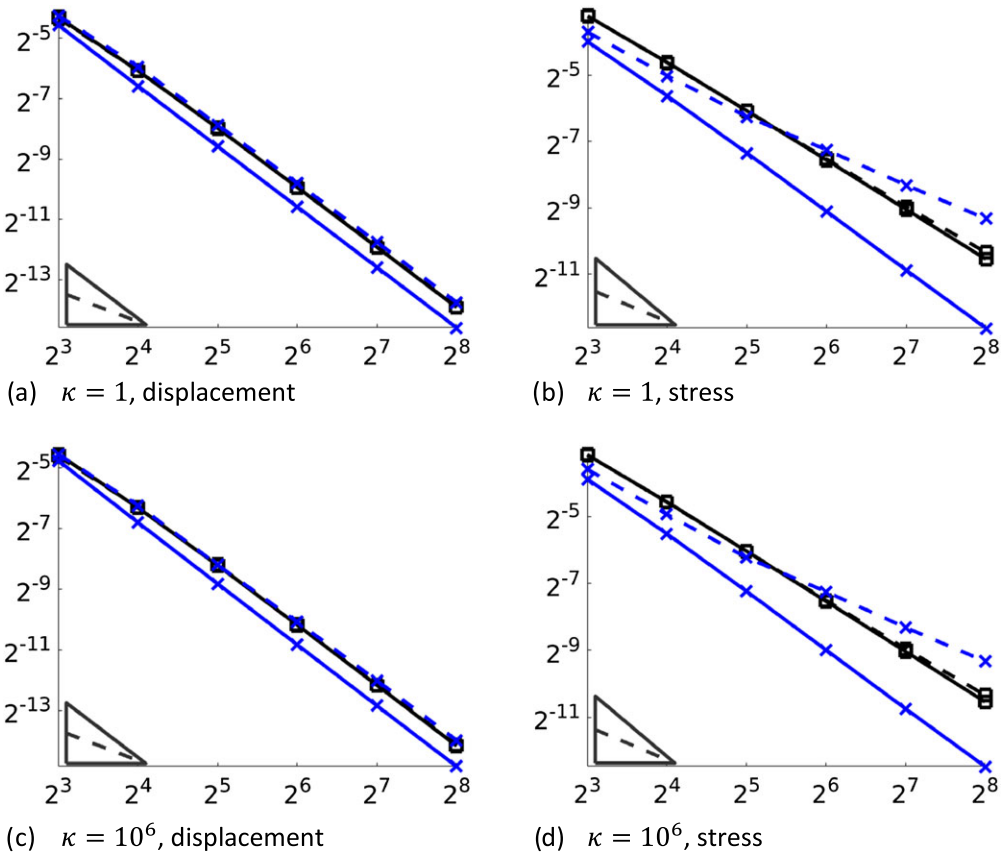

Figure 5. Convergence on Cartesian grids in 2D for homogeneous and heterogeneous medium. Legend: Black lines with squares represent MPSA-W, blue lines with crosses the generalized method, solid lines regular grids, and stippled lines perturbed grids. The axes show the square root of the number of degrees of freedom and the errors. Triangles indicate first-order (stippled) and second-order convergence. (a) $\kappa = 1$, displacement; (b) $\kappa = 1$, stress; (c) $\kappa = 10^6$, displacement; and (d) $\kappa = 10^6$, stress.

To quantify the errors, we compute the discrete L2 norm of the displacement error as

$$\epsilon_D = \frac{\left(\sum_{K\in\mathcal{T}} m_K \left(\boldsymbol{u}\left(\boldsymbol{x}_K\right) - \boldsymbol{u}_K\right)^2\right)^{\frac{1}{2}}}{\left(\sum_{K\in\mathcal{T}} m_K \boldsymbol{u}(\boldsymbol{x}_K)^2\right)^{\frac{1}{2}}} \tag{5.1.5}$$

Similarly, the error in stresses is given by

$$\epsilon_{\boldsymbol{\pi}} = \frac{\left(\sum_{\sigma\in\mathcal{F}} m_\sigma \left(\boldsymbol{\pi}\left(\boldsymbol{x}_\sigma\right) - \boldsymbol{\pi}_\sigma\right)^2\right)^{\frac{1}{2}}}{\left(\sum_{\sigma\in\mathcal{F}} m_\sigma \ \boldsymbol{\pi}(\boldsymbol{x}_\sigma)^2\right)^{\frac{1}{2}}} \tag{5.1.6}$$

5.1.2. Cartesian grids. Our first tests consider Cartesian grids. From Section 4, we expect both the generalized O-method and the new W-method to perform well in this case. Convergence results for 2D grids are reported in Figure 5. We observe that for regular grids, both methods are second order convergent in displacement, whereas the convergence rate for stress is reduced from roughly 1.5 on regular to first order on perturbed grids. We also observe that when a material heterogeneity is introduced by setting $\kappa = 10^6$, this has virtually no effect on the solution. In particular, the solutions show no sign of oscillations at the material interface.

DOI: 10.1002/nme

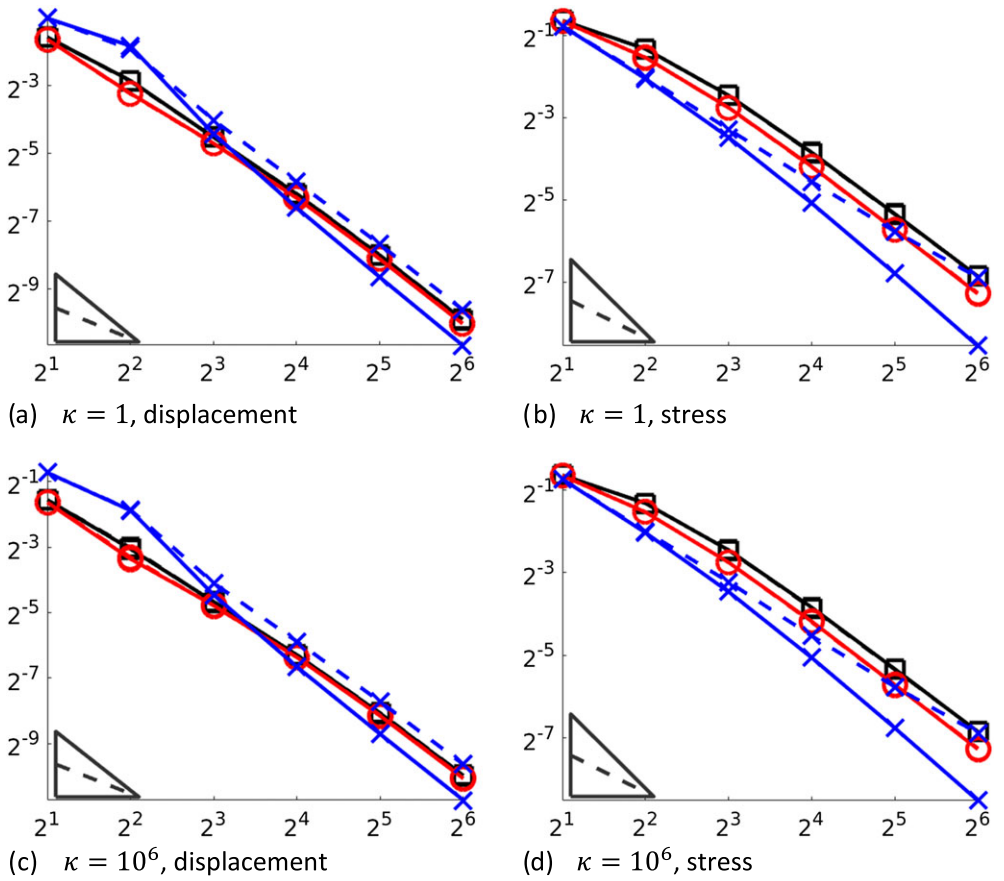

Figure 6. Convergence on Cartesian grids in 3D for homogenous and heterogeneous media. Legend: Black lines with squares represent MPSA-W with vertex-wise averaging, red lines with circles MPSA-W with edge-wise averaging, blue lines with crosses the O-method, solid lines regular grids, and stippled lines perturbed grids. The axes show the cubic root of the number of degrees of freedom and the errors. Triangles indicate first-order (stippled) and second-order convergence. (a) $\kappa = 1$, displacement; (b) $\kappa = 1$, stress; (c) $\kappa = 10^6$, displacement; and (d) $\kappa = 10^6$, stress.

Figure 6 shows the convergence behavior for the three-dimensional test case. Again, all methods exhibit second-order convergence in displacement; the generalized O-method has a slightly higher rate on unperturbed grids. The stresses have convergence rates of between 1.5 and 2 for unperturbed grids and between 1 and 1.5 on perturbed grids. We also see that for the W-method, edge-wise and vertex-wise averaging renders very similar results, although the edge-wise approach is slightly better. Again, a material heterogeneity has only minor impact on the quality of the solutions.

5.1.3. Simplex grids. Next, we consider the same test examples, but now on simplex grids. As mentioned in Section 4, the generalized MPSA-O method does not produce a coercive local problem for these grids, and the method may thus deteriorate. Conversely, the MPSA-W method is still coercive, and we expect better behavior of this method.

Figure 7 shows the convergence on triangular grids in 2D. The MPSA-W method yields second-order convergence in the displacement, and around 1.5 for the stresses. This holds for both perturbed and unperturbed grids. Comparison with the corresponding test on Cartesian grids reveals that the errors are roughly the same for similar numbers of degrees of freedom. As for Cartesian grids, the convergence is robust with respect to material heterogeneities. On regular grids, the combination of the grid pattern and the loss of coercivity cause the generalized O-method to produce a resonance error, resulting in only first-order convergence in displacement. Second-order convergence is recovered when the grid is perturbed.

DOI: 10.1002/nme

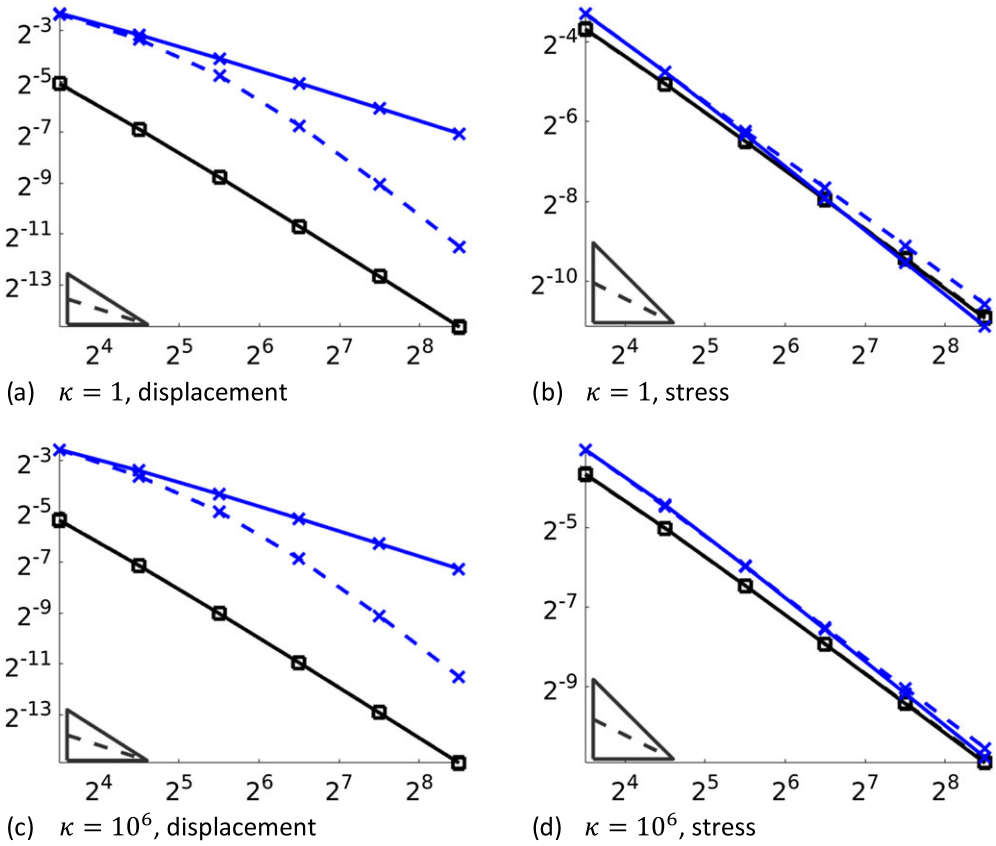

Figure 7. Convergence on simplex grids in 2D for homogeneous and heterogeneous medium. For legend, see Figure 5. (a) $\kappa = 1$, displacement; (b) $\kappa = 1$, stress; (c) $\kappa = 10^6$, displacement; and (d) $\kappa = 10^6$, stress.

We also remark that the simplex grids employed in this test are created by dividing squares, rendering right-angled triangles in the regular case. In additional tests on equilateral triangles (not shown here), we have observed that the generalized O-method may fail to converge at all. As noted in Section 4, the standard MPSA O-method with continuity point $1/3$ fulfills the local coercivity condition in this case and is therefore convergent. However, the standard O-method fails for local problems involving four cells meeting with right angles, creating a grid that is locally Cartesian. To apply the O-method on simplex grids in 2D, we therefore find it necessary either to require acute angles only or to switch between the standard and generalized methods depending on the local geometry. The MPSA-W method offers an attractive alternative that avoids these issues altogether.

For tetrahedral grids, the W-methods again perform well, with second-order convergence on displacements, and between first and second for stresses; see Figure 8. As for the Cartesian grids, edge-wise averaging consistently produces somewhat smaller errors; however, the difference is minor. The generalized O-method only slowly approaches its convergence region; on perturbed grids, the stresses do not converge for the grid refinements considered here. We observe that in this case, the material heterogeneity improves the convergence behavior.

While the generalized O-method is used as a benchmark herein, a comparison between the standard O-method and the lowest-order finite elements (FEM) was undertaken in [18]. For all cases considered therein, the O-method was at least as good as the FEM in terms of both displacements and stresses. We have not carried out a similar comparison here, but the experiments in this paper indicate that the MPSA-W method will also compare favorably with the FEM.

DOI: 10.1002/nme

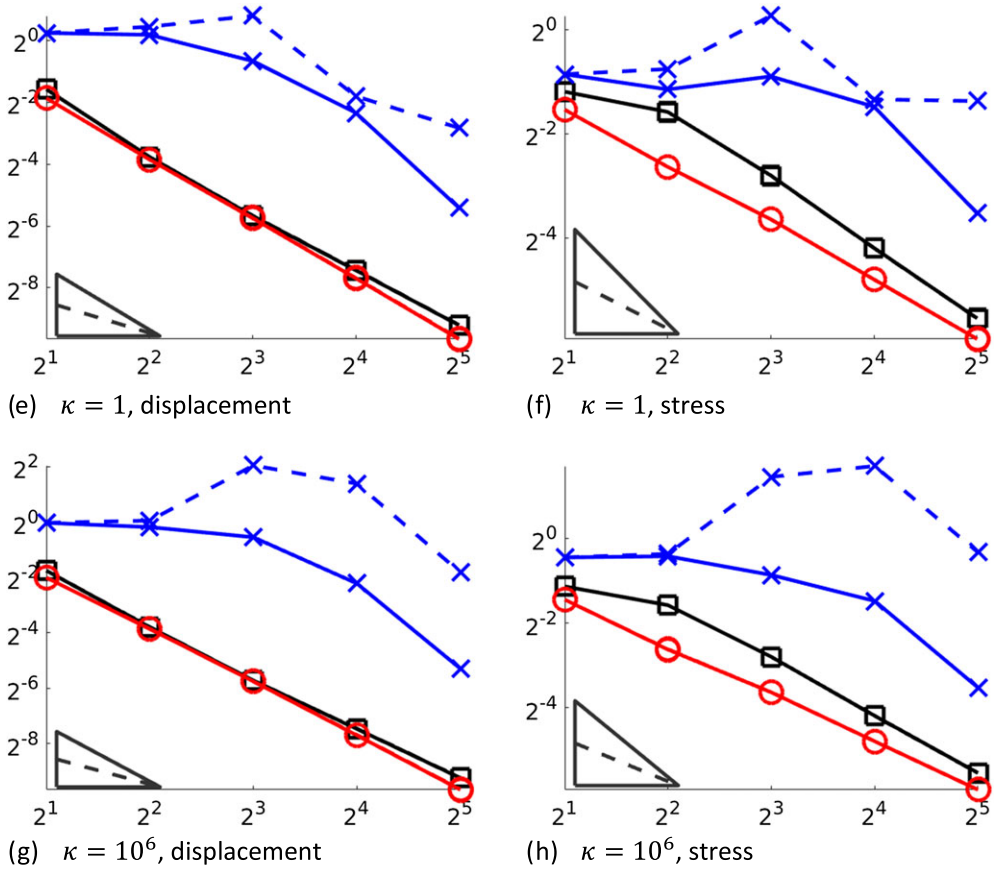

Figure 8. Convergence on simplex grids in 3D for homogeneous and heterogeneous medium. For legend, see Figure 6.(a) $\kappa = 1$, displacement; (b) $\kappa = 1$, stress; (c) $\kappa = 10^6$, displacement; and (d) $\kappa = 10^6$, stress.

5.1.4. Robustness to volume locking. The next test case considers convergence in the incompressible limit: both the 2D and 3D simulations with the ratio $\alpha = \lambda/\mu = \{10^2, 10^3, 10^4\}$, corresponding to Poisson's ratios $\nu = \lambda/(2(\lambda + \mu))$ of 0.495, 0.4995 and 0.49995, respectively. Only results from the 3D simulations are reported here; the 2D case showed a similar, although on average somewhat better, behavior. For simplicity, we consider a homogeneous domain; parameter heterogeneities did not alter the convergence properties.

These tests are potentially difficult for two reasons: First, low-order methods are known to suffer from volume locking in the incompressible limit. The MPSA methods have been shown to be free from volume locking for simplex grids [33], whereas for Cartesian grids, there is no proof that the methods will not exhibit locking. Second, for extreme parameter values combined with grid perturbations, the constant θ_2 in the local coercivity condition (Section 4.1) may not be bounded away from zero for all grid realizations, possibly leading to erratic convergence behavior.

Figure 9 depicts the convergence ratios on a Cartesian grid. We observe that for unperturbed grids, both displacement and stresses show steady convergence, with rates around 2 for displacement and around 1.5 for stresses. The generalized method yields a somewhat smaller error than the MPSA-W formulations, in particular for stresses. As the grid is perturbed, the displacement is still convergent, although with an irregular behavior for the O-method for the highest Poisson's ratio. The convergence rate for stresses is more sensitive to perturbations, in particular for the O-method. We have not seen signs of volume locking, and the irregular convergence behavior seems to be related to the constant θ in the local coercivity condition. We also note that for most of these cases, edge-wise and vertex-wise averaging of the stresses yields virtually indistinguishable results.

DOI: 10.1002/nme

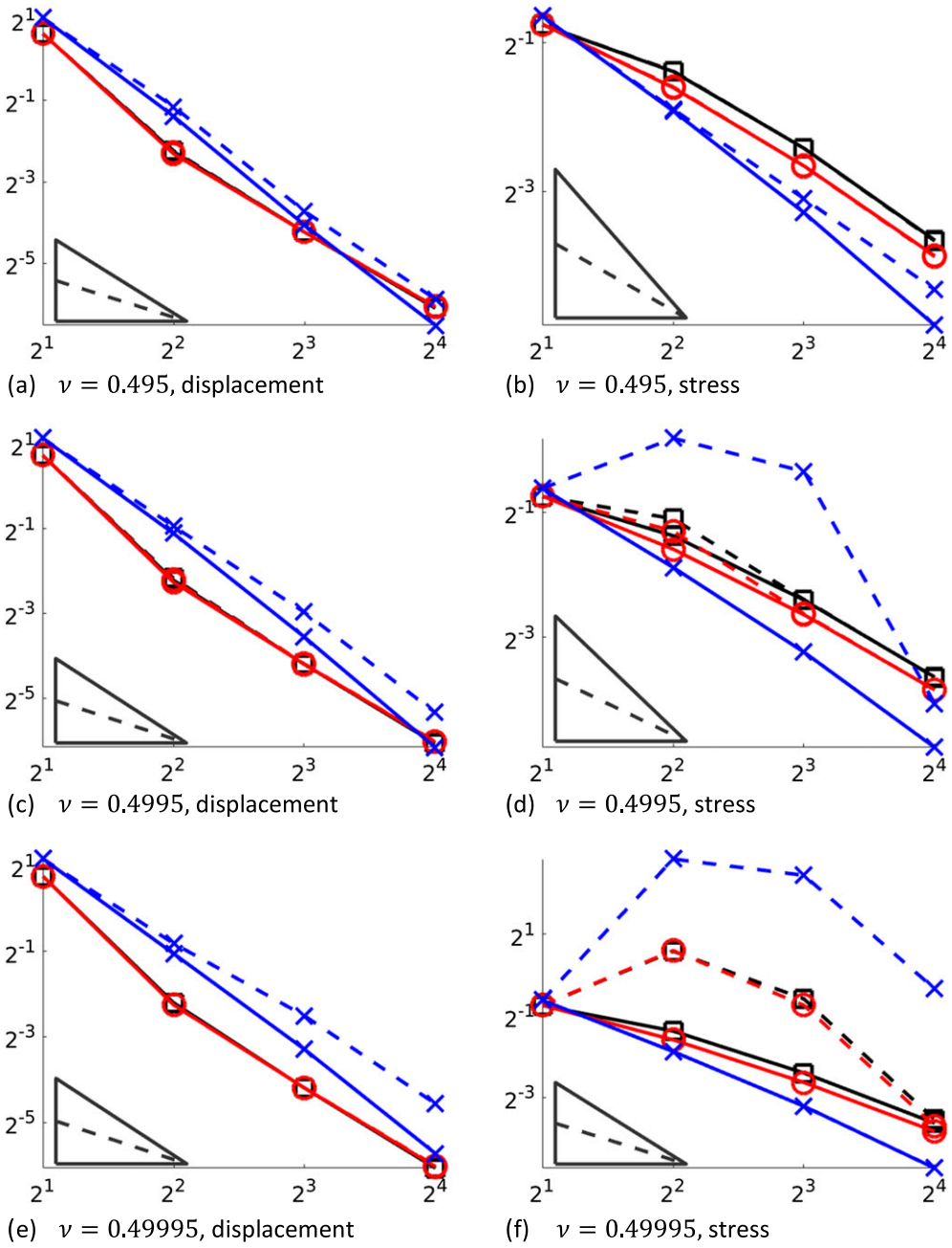

Figure 9. Homogeneous domain in 3D with Cartesian grid and increasing Poisson′s ratio. For legend, see Figure 6. (a) $\nu = 0.495$, displacement; (b) $\nu = 0.495$, stress; (c) $\nu = 0.4995$, displacement; (d) $\nu = 0.4995$, stress; (e) $\nu = 0.49995$, displacement; and (f) $\nu = 0.49995$, stress.

Next, we consider the performance on tetrahedral grids, shown in Figure 10. The convergence behavior is similar to that for Cartesian grids, for both unperturbed and perturbed grids. The methods obtain second-order convergence for displacement and first order for the stresses, independent of the Poisson's ratio. The only exception is for stresses on perturbed grids with high values of λ, where the MPSA-W methods show somewhat irregular convergence, and it is not clear whether O-method enters the region of convergence at all.

As a summary, the MPSA-W methods are more robust than the MPSA-O method, but all methods suffer from somewhat irregular convergence in stresses on perturbed grids for very high Poisson's

DOI: 10.1002/nme

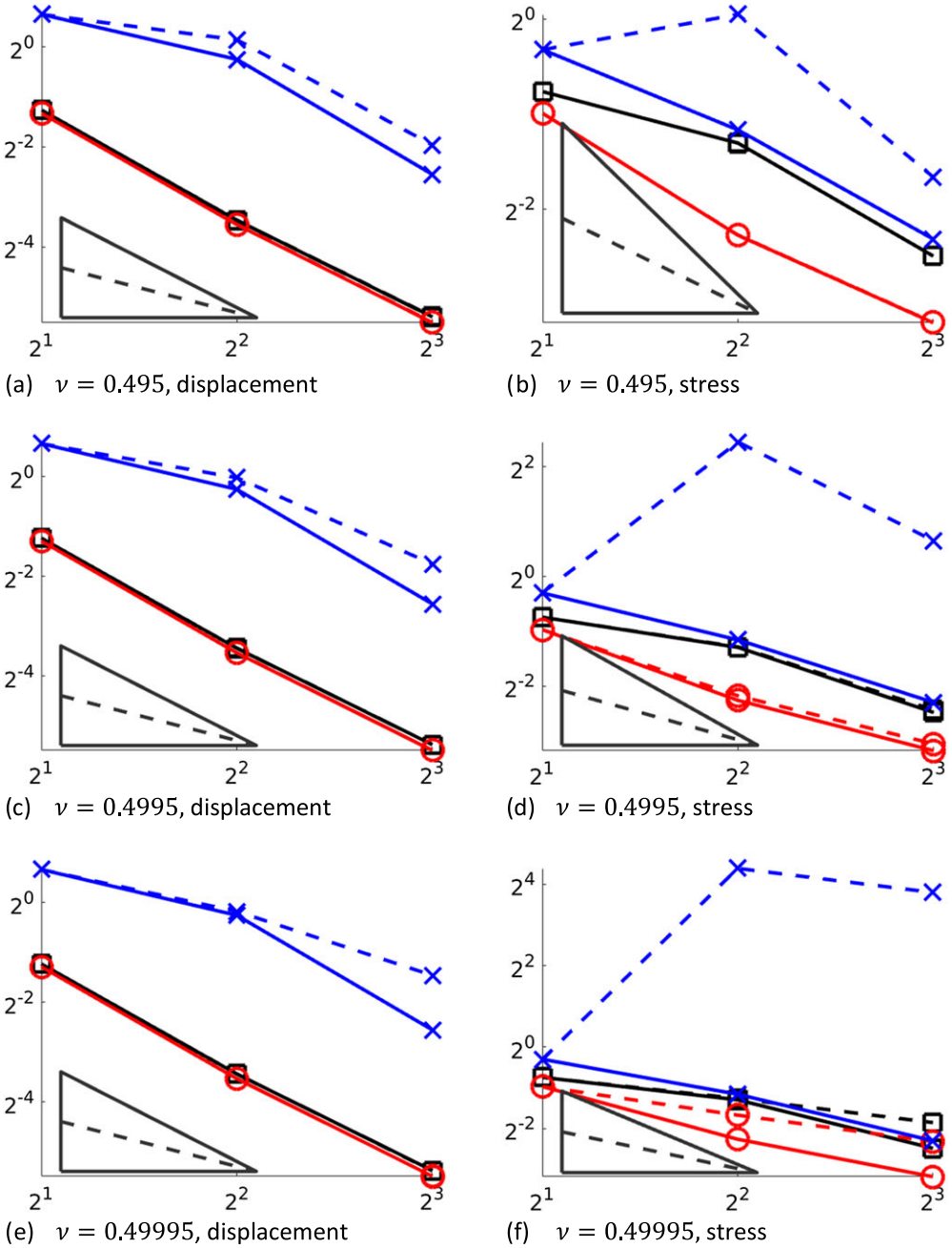

Figure 10. Homogeneous domain in 3D with tetrahedral grid and increasing Poisson's ratio. For legend, see Figure 6. (a) $\nu = 0.495$, displacement; (b) $\nu = 0.495$, stress; (c) $\nu = 0.4995$, displacement; (d) $\nu = 0.4995$, stress; (e) $\nu = 0.49995$, displacement; and (f) $\nu = 0.49995$, stress.

ratios. Additional simulations indicated that the irregularities are strongly connected to the magnitude of the grid perturbations. This also applies for simplex grids, where the MPSA methods are proven to be locking free. The erratic behavior thus seems to be related to the constant θ deteriorating: the combination of extreme parameters and grid perturbations, which for some grid realizations bring the methods outside their region of convergence.

5.1.5. Coupling with solid pressure. As for traditional FEMs, the MPSA-W methods can be stabilized in the incompressible limit by the introduction of a solid pressure [52], denoted p and defined

DOI: 10.1002/nme

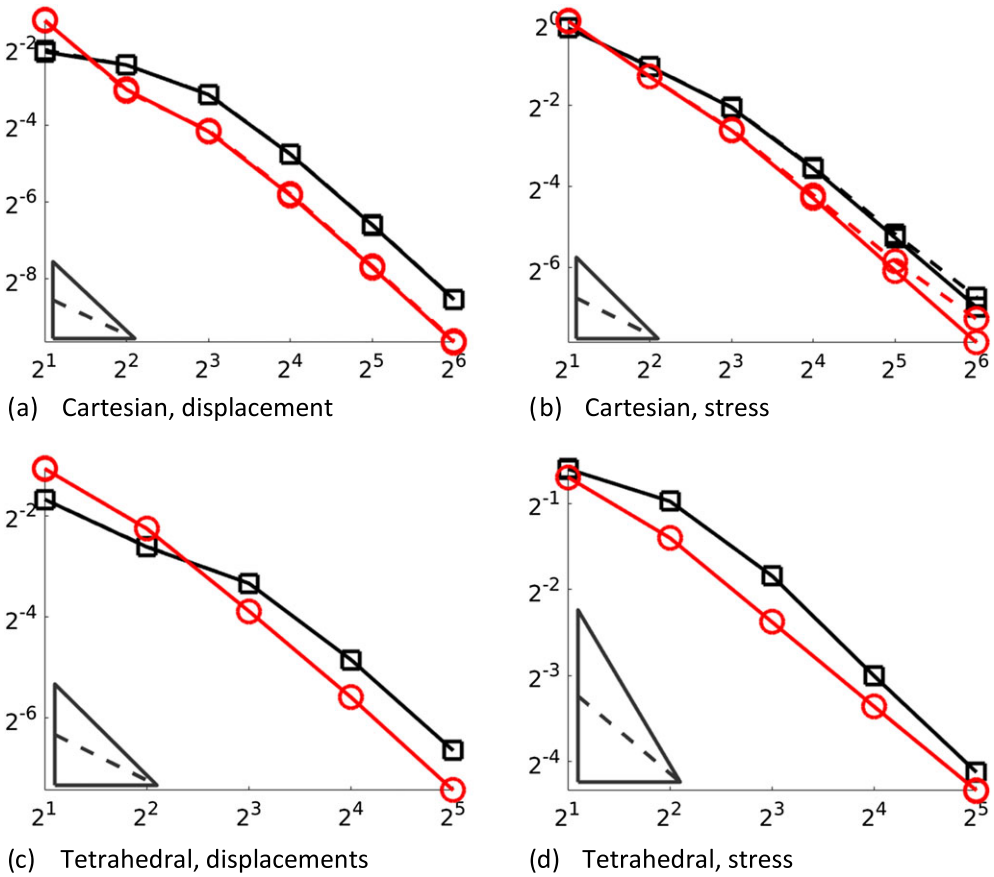

Figure 11. Convergence for MPSA-W on Cartesian and simplex grids in 3D, obtained with a solid pressure formulation. The Poisson's ratio is set to $\nu = 0.49995$. Legend: Black lines with squares represent MPSA-W with vertex-wise averaging, red lines with circles MPSA-W with edge-wise averaging, solid lines regular grids, and stippled lines perturbed grids. Triangles indicate first-order (stippled) and second-order convergence. (a) Cartesian, displacement; (b) Cartesian, stress; (c) tetrahedral, displacement; and (d) tetrahedral, stress.

at the cell centers, and solve the mixed system

$$\nabla \cdot (2\mu\boldsymbol{\epsilon} - pI) = \boldsymbol{f} \tag{5.1.7}$$

$$\nabla \cdot tr\,(\boldsymbol{\epsilon}) + \frac{p}{\lambda} = 0 \tag{5.1.8}$$

The system (5.1.7) to (5.1.8) has the same structure as Biot's equations for poro-elastic media, with $1/\lambda$ interpreted as the fluid compressibility, and with a zero permeability. As noted in the introduction, the MPSA method has been extended to Biot's equations [21], and we use that approach to discretize the coupling terms $\nabla \cdot (pI)$ and $\nabla \cdot tr\,(\boldsymbol{\epsilon})$. Crucially, for this example, the discretization has been shown to be stable, independent of λ; see [21] for details

Figure 11 shows the convergence of the resulting methods for a Poisson's ratio of $\nu = 0.49995$; the results for lower ratios were practically identical. We observe close to second-order convergence for displacements and between the first and second orders for stresses. However, the convergence issues are to some extent transferred to the solid pressures p, as can be seen in Figure 12, in that on simplex grids, the convergence rate only slowly reaches first order. On Cartesian grids, the solid pressure is again first order convergent on perturbed grids and displays an unexpected super-convergence in the sense of second-order convergence on smooth grids. While the solid pressure makes the W-methods

DOI: 10.1002/nme

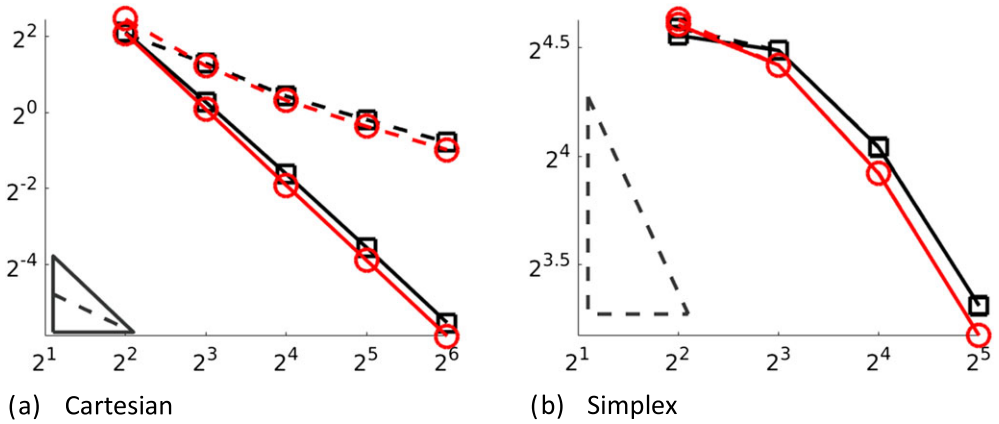

Figure 12. Convergence for the solid pressure p using MPSA-W on Cartesian (a) and simplex (b) grids in 3D, obtained with a solid pressure formulation. The Poisson's ratio is set to $\nu = 0.49995$. For legend, see Figure 11.

robust with respect to grid perturbations, it does not have a similar effect on the O-method, which retains its erratic behavior (not shown). This further indicates that the convergence issues for the MPSA O-method are not related to traditional locking.

We note that the discretization of the solid pressure is identical to the MPSA discretization for Biot's equations in the limit of zero fluid compressibility and rock permeability. Indeed, although poro-elastic systems are outside the scope of this paper, we have verified that similar to MPSA-O, the weakly symmetric method can be extended to poro-elasticity by applying the same steps as introduced in [21].

5.2. *Angular momentum*

The MPSA W-method imposes symmetry of stress weakly; however, it is important to note that a strongly symmetric stress tensor can always be recovered. Indeed, every finite volume method provides balanced tractions on the faces of the grid, and a symmetric point-wise stress tensor is thus obtained using any finite element space for stress with strong symmetry as an interpolant (e.g., Arnold–Winther elements on simplexes [34]). This post-processed stress tensor will be locally symmetric for both the MPSA-O and MPSA-W methods.

A related question is whether the weak symmetry impacts the convergence rate of the rotational components of the stress. As a final test of the method, we therefore consider the angular momentum of the surface forces on each cell. Denote by $\boldsymbol{T}^t_{K,\sigma}$ the tangent component of the stresses on surface σ, as seen from cell K. The angular momentum of $\boldsymbol{T}^t_{K,\sigma}$ around the cell center is given by $\Omega_{K,\sigma} = \boldsymbol{T}^t_{K,\sigma} \times (\boldsymbol{x}_\sigma - \boldsymbol{x}_K)$, and the total angular momentum on K is $\Omega_K = \sum_{\sigma \in \mathcal{F}_K} \Omega_{K,\sigma}$. We then measure the quality of the approximated angular momentum by the mean of the absolute value over all cells in the grid.

Two metrics were considered for the angular momentum: First, because of symmetry of the stress tensor, under grid refinement, the angular momentum should converge with a rate of more than h^D (h being the grid diameter) in analogue to the second Cauchy stress theorem. This convergence was verified for all cases considered. Second, we measured the difference in angular momentum between the numerical and analytical surface stresses. Figure 13 shows the convergence of this quantify for the 2D and 3D test problems with a homogenous domain ($\kappa = 1$). The angular momentum for both the O-method and the W-method converges with a rate of above 3, and despite the weakly imposed symmetry, the W-method is as accurate as the O-method.

DOI: 10.1002/nme

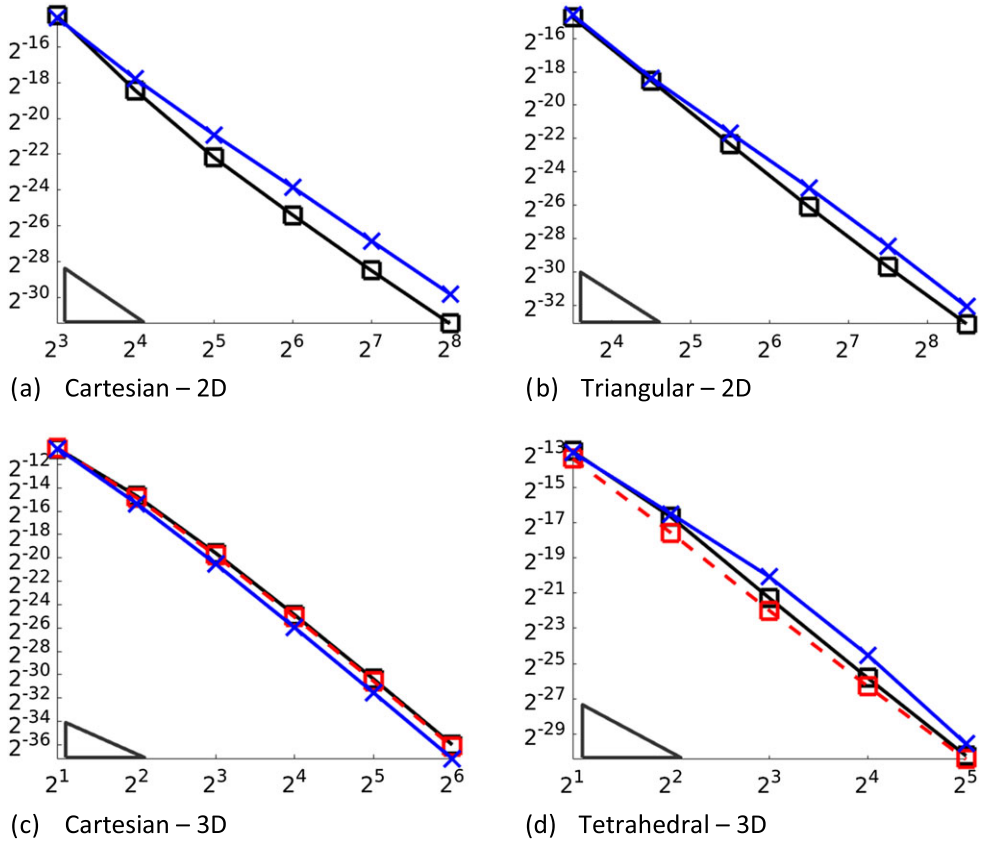

Figure 13. Difference between analytical and numerical angular momentum around cell centers, taken as the mean value over all cells. Legend: W-method node-wise in black squares, W-method edge-wise in red squares (only 3D), and O-method in black crosses. The axes show square (2D) or cubic (3D) root of the number of degrees of freedom and the errors. Triangles indicate third-order convergence. (a) Cartesian, 2D; (b) triangular, 2D; (c) Cartesian, 3D; and (d) tetrahedral, 3D.

5.3. *Computational cost*

The main computational cost in the discretization is related to the inversion of the linear system (3.3.4). Here, the MPSA-W methods give a significant computational saving compared with the generalized approach: First, the number of displacement continuity points is significantly reduced. This is particularly important in 3D, where the number of displacement continuity equations is reduced from 144 to 36 for Cartesian grids and on average from about 360 to 90 for simplex grids considered herein. Second, in the weakly symmetric formulation, the linear system is no longer overdetermined, and it can be solved as a direct problem, rather than a constrained optimization problem.

The MPSA methods considered herein all lead to the same cell stencils and can be expected to have a similar cost in solving the global linear system. While a systematic investigation is beyond the scope of this paper, it is our experience that when iterative solvers are employed, specifically GMRES with ILU and AMG preconditioners, the number of iterations are roughly the same for all methods. The exception is the O-method on simplex grids, where 2–4 times more iterations may be needed. Again, we suspect that this is related to a lack of local coercivity.

6. CONCLUDING REMARKS

In this paper, we have introduced a weakly symmetric finite volume method for elasticity, termed the W-method. The method uses cell-centered variables, and when combined with the ideas introduced in [21], it is particularly well suited for simulations of coupled flow and deformation in porous media.

DOI: 10.1002/nme

The MPSA-W method differs from previous MPSA methods in that it is robust on both simplex and Cartesian grids and that it has a lower computational cost.

Convergence of the W-method was shown by casting the method in a discrete variational form previously established for the MPSA-O method. The convergence criteria, which depend only on the grid and the constitutive law, can be verified at the time of discretization. While both the W-method and the O-method are convergent on Cartesian grids, only the W-method has this property also on simplex grids, whereas the O-method loses local coercivity.

We present an extensive suite of numerical experiments, including the first comprehensive convergence tests for the MPSA methods in 3D. Both the W-method and the O-method performed well on Cartesian grids, but only the W-method showed similar behavior on simplex grids. While the weak symmetry in the W-method in 3D can be imposed by vertex-wise or edge-wise averaging, the numerical experiments further indicated that the extra accuracy obtained by the edge-wise approach does not justify the additional data structure needed, and thus, vertex-wise averaging is the preferred version of the method.

This work has been limited to linear discretizations; however, we expect that the approach will extend to more general constitutive models, under the condition that the stress can be given as an explicit function of the material deformation. However, it is clear that for materials and problems wherein there is plastic deformation, additional concepts will be needed. An extended discussion of how methods of this class can be extended to complex constitutive laws is reported in [53].

The results reported herein allow us to conclude that the new MPSA-W method represents the most simple, efficient, and robust version of the MPSA methods currently available and forms the benchmark for future developments of the methods.

ACKNOWLEDGMENTS

The first author was funded by the Research Council of Norway through grant no. 228832/E20 and Statoil ASA through the Akademia agreement.

REFERENCES

1. Rutqvist J. The geomechanics of CO2 storage in deep sedimentary formations. *Geotechnical and Geological Engineering* 2012; **30**(3):525–551.
2. Fakcharoenphol P, Xiong Y, Hu L, Winterfeld PH, Xu T, Wu Y-S. USER'S GUIDE of TOUGH2-EGS-MP: a massively parallel simulator with coupled geomechanics for fluid and heat flow in enhanced geothermal systems, 2013.
3. Pettersen Ø, Kristiansen TG. Improved compaction modeling in reservoir simulation and coupled rock mechanics/flow simulation, with examples from the Valhall field. *SPE REE* 2009; **12**(2):329–340.
4. Chen Z, Huan G, Ma Y. *Computational Methods for Multiphase Flows in Porous Media*, 2006.
5. Zienkiewicz OC, Taylor RL. The finite element method: The basis. Volume 1. 5th edition 2000 Butterworth-Heinemann. vol. 1, 2000; 708.
6. Schlumberger, Eclipse Manual, 2010.
7. Haga JB, Osnes H, Langtangen HP. On the causes of pressure oscillations in low-permeable and low-compressible porous media. *International Journal for Numerical and Analytical Methods in Geomechanics* 2012; **36**(12):1507–1522.
8. Scovazzi G, Carnes B, Zeng X, Rossi S. A simple, stable, and accurate linear tetrahedral finite element for transient, nearly, and fully incompressible solid dynamics: a dynamic variational multiscale approach. *International Journal for Numerical Methods in Engineering* 2016; **106**(10):799–839.
9. Gaspar FJ, Lisbona FJ, Oosterlee CW. A stabilized difference scheme for deformable porous media and its numerical resolution by multigrid methods. *Computing and Visualization in Science* 2008; **11**(2):67–76.
10. OpenFOAM Foundation, OpenFOAM Documentation. Available from https://www.openfoam.org/docs/, 2014.
11. Lee D, Cardiff P, Bryant EC, Manchanda R, Wang H, Sharma MM. A new model for hydraulic fracture growth in unconsolidated sands with plasticity and leak-off. In *Proceedings of SPE Annual Technical Conference and Exhibition*, 2015.
12. Cardiff P, Manchanda R, Bryant EC, Lee D, Ivankovich A, Sharma MM. Simulation of fractures in OpenFOAM: from adhesive joints to hydraulic fractures. In Proceedings of In *10th OpenFOAM Workshop*, 2015.
13. Aziz K, Settari A. *Petroleum Reservoir Simulation*. Applied Science Publishers: Philadelphia, 1979.
14. Edwards MG, Lazarov RD, Yotov I. Special issue on locally conservative numerical methods for flow in porous media. *Computers & Geosciences* 2002; **4**:3–4.
15. Christie MA, Blunt MJ. Tenth SPE comparative solution project: a comparison of upscaling techniques. *SPE Reservoir Evaluation & Engineering* 2001; **4**:308–317.
16. Eymard, R., Hérard J-M. *Finite Volumes for Complex Applications V. ISTE Limited*, 2008.

DOI: 10.1002/nme

17. Sword C, Mallison B, Milliken W. Unstructured cut-cell grids for modeling complex reservoirs. In *Proceedings of the 21st SPE Reservoir simulation symposium*. 2013.
18. Nordbotten JM. Cell-centered finite volume discretizations for deformable porous media. *International Journal for Numerical Methods in Engineering* 2014; **100**(6):399–418.
19. Computer Modeling Group LLC, GEM: generalized equation-of-state model compositional reservoir simulation. 2015.
20. Flemisch B,. et al. DuMux: DUNE for multi-{phase,component,scale,physics,...}flow and transport in porous media. *Advances in Water Resources* 2011; **34**(9):1102–1112.
21. Nordbotten JM. Stable cell-centered finite volume discretization for Biot equations. *SIAM Journal on Numerical Analysis* 2016; **54**(2):942–968.
22. Demirdžić I. A fourth-order finite volume method for structural analysis. *Applied Mathematical Modelling* 2016; **40**(4):3104–3114.
23. Jasak H, Weller HG. Application of the finite volume method and unstructured meshes to linear elasticity. *International Journal for Numerical Methods in Engineering* 2000; **48**:267–287.
24. Cardiff P, Tuković HJ, Ivanković A. A block-coupled finite volume methodology for linear elasticity and unstructured meshes. *Computers & Structures* 2016; **175**:100–122.
25. Tuković Ž, Ivanković A, Karač A. Finite-volume stress analysis in multi-material linear elastic body. *International Journal for Numerical Methods in Engineering* 2013; **93**(4):400–419.
26. Voller VR. *Basic Control Volume Finite Element Methods for Fluids and Solids*, 2009.
27. Kluth G, Despres B. Discretization of hyperelasticity on unstructured mesh with a cell-centered Lagrangian scheme. *Journal of Computational Physics* 2010; **229**(24):9092–9118.
28. Lee CH, Gil AJ, Bonet J. Development of a cell centred upwind finite volume algorithm for a new conservation law formulation in structural dynamics. *Computers & Structures* 2013; **118**:13–38.
29. Arnold DN, Falk RS, Winther R. Mixed finite element methods for linear elasticity with weakly imposed symmetry. *Mathematics of Computation* 2007; **76**(260):1699–1724.
30. Nguyen NC, Peraire J. Hybridizable discontinuous Galerkin methods for partial differential equations in continuum mechanics. *Journal of Computational Physics* 2012; **231**(18):5955–5988.
31. Di Pietro DA, Lemaire S. An extension of the Crouzeix–Raviart space to general meshes with application to quasi-incompressible linear elasticity and Stokes flow. *Mathematics of Computation* 2014; **84**(291):1–31.
32. Di Pietro DA, Ern A. A hybrid high-order locking-free method for linear elasticity on general meshes. *Computer Methods in Applied Mechanics and Engineering* 2015; **283**:1–21.
33. Nordbotten JM. Convergence of a cell-centered finite volume discretization for linear elasticity. *SIAM Journal on Numerical Analysis* 2015; **53**(6):2605–2625.
34. Arnold DN, Winther R. Mixed finite elements for elasticity. *Numerische Mathematik* 2002; **92**(3):401–419.
35. Beirão Da Veiga L. A mimetic discretization method for linear elasticity. *ESAIM Mathematical Modelling and Numerical Analysis* 2010; **44**(2):231–250.
36. Aavatsmark I. An introduction to multipoint flux approximations for quadrilateral grids. *Computers & Geosciences* 2002; **6**(3/4):405–432.
37. Klausen RA, Radu FA, Eigestad GT. Convergence of MPFA on triangulations and for Richards' equation. *International Journal for Numerical Methods in Fluids* 2008; **58**(12):1327–1351.
38. Jenny P, Lee S, Tchelepi HA. Multi-scale finite-volume method for elliptic problems in subsurface flow simulation. *Journal of Computational Physics* 2003; **187**(1):47–67.
39. Nordbotten JM, Bjørstad PE. On the relationship between the multiscale finite-volume method and domain decomposition preconditioners. *Computers & Geosciences* 2008; **12**(3):367–376.
40. Agélas L, Guichard C, Masson R. Convergence of finite volume MPFA O type schemes for heterogeneous anisotropic diffusion problems on general meshes. *International Journal On Finite Volumes* 2010; **7**(2).
41. Eymard R, Gallouët T, Herbin R. A new finite volume scheme for anisotropic diffusion problems on general grids: convergence analysis. *Comptes Rendus de L'Académie des Sciences - Series I* 2007; **344**:403–406.
42. Hughes TJR, Feijóo GR, Mazzei L, Quincy J-B. The variational multiscale method—a paradigm for computational mechanics. *Computer Methods in Applied Mechanics and Engineering* 1998; **166**(1–2):3–24.
43. Aavatsmark I, Eigestad GT, Klausen RA. *Numerical Convergence of the MPFA O-method for General Quadrilateral Grids in Two and Three Dimensions*, vol. 142. Springer New York: New York, NY, 2006.
44. Klausen RA, Winther R. Robust convergence of multi point flux approximation on rough grids. *Numerische Mathematik* 2006; **104**(3):317–337.
45. Faigle B, Helmig R, Aavatsmark I, Flemisch B. Efficient multiphysics modelling with adaptive grid refinement using a MPFA method. *Computers & Geosciences* 2014; **18**(5):625–636.
46. Hansbo P, Larson MG. Discontinuous Galerkin methods for incompressible and nearly incompressible elasticity by Nitsche's method. *Computer Methods in Applied Mechanics and Engineering* 2002; **191**(17–18):1895–1908.
47. Brenner SC. Korn's inequalities for piecewise H1 vector fields. *Mathematics of Computation* 2003; **73**(247):1067–1087.
48. Wheeler MF, Yotov I. A multipoint flux mixed finite element method. *SIAM Journal on Numerical Analysis* 2006; **44**(5):2082–2106.
49. Klausen RA, Russell TF. Relationships among some locally conservative discretization methods which handle discontinuous coefficients. *Computers & Geosciences* 2005; **8**(4):341–377.

DOI: 10.1002/nme

50. Russell TF, Wheeler MF. Finite element and finite difference methods for continuous flows in porous media. In *The Mathematics of Reservoir Simulation*, Ewing RE (ed.). SIAM: Philadelphia, 1983.
51. Finite Volume Methods for Biot's equations. Available from: www.github.com/keileg/fvbiot, 2016.
52. Hughes TJR. *The Finite Element Method: Linear Static and Dynamic Finite Element Analysis*, 1987.
53. Keilegavlen E, Nordbotten JM, Stephansen AF. Tensor relative permeabilities: origins, modeling and numerical discretization. *International Journal of Numerical Analysis and Modeling* 2012; **9**(3):701–724.

DOI: 10.1002/nme